Passivity Enforcement via Perturbation of Hamiltonian Matrices

Passivity Enforcement via Perturbation of Hamiltonian Matrices

Stefano Grivet-Talocia, *Member, IEEE*

***Abstract*—This paper presents a new technique for the passivity enforcement of linear time-invariant multiport systems in state-space form. This technique is based on a study of the spectral properties of related Hamiltonian matrices. The formulation is applicable in case the system input-output transfer function is in admittance, impedance, hybrid, or scattering form. A standard test for passivity is first performed by checking the existence of imaginary eigenvalues of the associated Hamiltonian matrix. In the presence of imaginary eigenvalues the system is not passive. In such a case, a new result based on first-order perturbation theory is presented for the precise characterization of the frequency bands where passivity violations occur. This characterization is then used for the design of an iterative perturbation scheme of the state matrices, aimed at the displacement of the imaginary eigenvalues of the Hamiltonian matrix. The result is an effective algorithm leading to the compensation of the passivity violations. This procedure is very efficient when the passivity violations are small, so that first-order perturbation is applicable. Several examples illustrate and validate the procedure.**

***Index Terms*—Hamiltonian matrices, linear macromodeling, passivity, perturbation theory.**

I. Introduction

THE RESEARCH that motivates this work is focused on the generation of linear lumped macromodels for multiport interconnects. Such macromodels are of paramount importance for the analysis and design of any high-speed electronic system. In fact, the signal integrity (SI) of such systems can only be assessed by accurate system-level simulations including suitable models for all the parts of the system that have some influence on the signals. It is well known that electrical interconnects such as packages, vias, and discontinuities in general may strongly affect the SI if the design is poor. Therefore, accurate models for such structures must be derived and connected one to each other in order to perform system-level SI analyzes. This latter stage may lead to serious instabilities if the single macromodels are nonpassive. In fact, it is well known that stable but nonpassive structures may become unstable depending on the termination networks.

The standard procedure for the generation of lumped macromodels is to derive some rational approximation of the transfer matrix for the structure under investigation. A large number of publications have recently appeared, focusing on various approaches to this rational approximation problem. The reader is referred to [6], [8], [12], [16], [10] (this list only illustrative) and references therein. Some methods start from large circuit descriptions of the structure and perform some model order reduction for the derivation of reduced complexity macromodels. These methods, usually based on Krylov subspace techniques and congruent transformations, guarantee the passivity of the macromodels if the original circuit description is passive. Unfortunately, such a circuit description may not always be available. Therefore, alternative approaches have been proposed for the identification of lumped macromodels starting from input-output port responses, either in time or frequency domain. Although very accurate approximations can be generated even for quite complex structures, the typical outcome of such methods is a stable but possibly nonpassive model. This paper intends to propose a technique for the detection and compensation of passivity violations for such macromodels.

Passivity may be defined in a loose sense as the inability of a given structure to generate energy. The precise definition of passivity [2] requires that the transfer matrix under investigation be positive real (in case of hybrid representations of the multiport) or bounded real (in case of scattering representations). The direct application of these definitions for testing passivity, however, requires a frequency sweep since these conditions need to be checked at any frequency [13], [7]. The results of such tests, therefore, depend on an accurate sampling of the frequency axis, which is not a trivial task [19]. Erroneous results may occur. For this reason, purely algebraic passivity tests are highly desirable [17].

Fortunately, the positive real lemma and the bounded real lemma provide an answer to this problem [4]. These results provide a connection between the passivity definitions and various equivalent algebraic conditions. These conditions can be expressed via feasibility of linear matrix inequalities (LMI), or via existence of solutions to equivalent algebraic Riccati equations (ARE), or via the spectral properties of associated Hamiltonian matrices. For an excellent review and a rich bibliography on the subject, we refer the reader to [4]. In this paper, we focus on the latter formulation using Hamiltonian matrices, since a study of their spectral properties leads not only to a precise criterion for passivity check, but also to a simple algorithm for the passivity compensation in case some passivity violations are detected. We remark that the investigated problem has several connections in partially related fields of application, including optimal control [24]. However, the main results will be presented under the perspective of macromodeling, without making connections to other possible applications. This paper gives a de-

Manuscript received May 20, 2003; revised March 23, 2004. This work was supported in part by the Italian Ministry of University (MIUR) under the Program for the Development of Research of National Interest Grant 2002093437, and in part by Center for Multimedia Radio Communications (CERCOM), Department of Electronics, Polytechnic University of Turin. This paper was recommended by Associate Editor S. C. Dutta Roy.

The author is with the Department of Electronics, Polytechnic University of Turin, 10129 Turin, Italy (e-mail: grivet@polito.it).

Digital Object Identifier 10.1109/TCSI.2004.834527

tailed formulation for the preliminary results presented in [9]. An alternative passivity compensation algorithm also based on Hamiltonian matrices is described in [20].

The outline of this paper is as follows. First, the notations and the background material will be detailed in Section II. Section III will present the main results for the characterization of passivity violations. These results will be summarized in two algorithms for the precise characterization of local passivity violations for hybrid (including impedance and admittance) and scattering representations. These algorithms are based on application of first-order perturbation theory to the imaginary eigenvalues of the associated Hamiltonian matrices. Section IV will describe a procedure for the passivity enforcement. Also in this case, the first-order perturbation theory will be applied, but as an inverse problem. The perturbation of the original system that is necessary for a suitable modification of the spectrum of the associated Hamiltonian matrices will be computed. An iterative perturbation algorithm will be designed for the automatic passivity compensation. Section V will present several validations and application examples.

II. Preliminary and Notations

In this section, we set the notations, we recall the known background material that will be used throughout this work, and we highlight the working hypotheses that are needed for the derivation of the main results.

A. Basic Vector and Matrix Notations

Throughout this paper, we use boldface lowercase fonts, e.g., $\boldsymbol{x}$, to denote vectors and boldface uppercase fonts, e.g., $\boldsymbol{Z}$, to denote matrices. The identity matrix will be denoted as $\boldsymbol{I}$, with a size to be defined by the context. Similarly, a matrix with vanishing entries will be denoted as $\boldsymbol{0}$. For a generic complex matrix $\boldsymbol{Z}$, we will denote with $\boldsymbol{Z}^*$ its complex conjugate, with $\boldsymbol{Z}^T$ its transpose, and with $\boldsymbol{Z}^H$ its complex conjugate transpose. With $\lambda(\boldsymbol{Z})$, we denote the set of all eigenvalues of $\boldsymbol{Z}$, whereas $\sigma(\boldsymbol{Z})$ indicates the set of its singular values. We recall that the singular values are characterized as

$$\sigma_0 \geq 0 \in \sigma(\boldsymbol{Z}) \iff \sigma_0^2 \in \lambda(\boldsymbol{Z}^H\boldsymbol{Z})\,. \tag{1}$$

The Kronecker matrix product [22] will be a useful tool for the formulation of the passivity compensation algorithm. Given a $p\times q$ matrix $\boldsymbol{A}$ and an arbitrary matrix $\boldsymbol{B}$, the Kronecker product is defined as

$$\boldsymbol{A}\otimes\boldsymbol{B} = \begin{pmatrix} a_{11}\boldsymbol{B} & \cdots & a_{1q}\boldsymbol{B} \\ \vdots & & \vdots \\ a_{p1}\boldsymbol{B} & \cdots & a_{pq}\boldsymbol{B} \end{pmatrix}. \tag{2}$$

A useful property of the Kronecker product is the following equivalence, for suitable matrices for which the products make sense:

$$\boldsymbol{Y} = \boldsymbol{B}\boldsymbol{X}\boldsymbol{A}^T \quad\Longleftrightarrow\quad \mathrm{vec}(\boldsymbol{Y}) = (\boldsymbol{A}\otimes\boldsymbol{B})\mathrm{vec}(\boldsymbol{X}) \tag{3}$$

where the notation $\mathrm{vec}(\boldsymbol{X})$ denotes the a vector storing the stacked columns of matrix $\boldsymbol{X}$. This equivalence is useful to restate in explicit form the linear constraint between the matrices $\boldsymbol{Y}$ and $\boldsymbol{X}$ on the left. Note that the following equivalence holds between the Frobenius norm of $\boldsymbol{X}$ and the Euclidean norm of $\mathrm{vec}(\boldsymbol{X})$:

$$\|\boldsymbol{X}\|_F^2 = \mathrm{tr}(\boldsymbol{X}\boldsymbol{X}^H) = \mathrm{tr}(\boldsymbol{X}^H\boldsymbol{X}) = \sum_{i,j}|X_{ij}|^2 = \|\mathrm{vec}(\boldsymbol{X})\|_2^2 \tag{4}$$

where $\mathrm{tr}(\cdot)$ denotes the trace, i.e., the sum of the diagonal elements of its argument.

B. Hamiltonian Matrices

We will need the following basic facts on real Hamiltonian matrices. More details can be found, e.g., in [3], [15], [4] and references therein. A matrix $\boldsymbol{M}\in\mathbb{R}^{2n\times 2n}$ is Hamiltonian if

$$\boldsymbol{J}^{-1}\boldsymbol{M}\boldsymbol{J} = -\boldsymbol{M}^T \tag{5}$$

where

$$\boldsymbol{J} = \begin{pmatrix} \boldsymbol{0} & \boldsymbol{I} \\ -\boldsymbol{I} & \boldsymbol{0} \end{pmatrix}. \tag{6}$$

Note that $\boldsymbol{J}^{-1} = \boldsymbol{J}^T = -\boldsymbol{J}$. If $\lambda_0\in\lambda(\boldsymbol{M})$ is an eigenvalue of $\boldsymbol{M}$, then also $-\lambda_0\in\lambda(\boldsymbol{M})$, since the characteristic polynomial is real and even. Therefore, the spectrum of $\boldsymbol{M}$ is symmetric with respect to both real and imaginary axis. Let $\boldsymbol{w}_+$ and $\boldsymbol{v}_+$ be the left and right eigenvectors associated to some eigenvalue λ_0,

$$\boldsymbol{M}\boldsymbol{v}_+ = \lambda_0\boldsymbol{v}_+, \quad \boldsymbol{M}^T\boldsymbol{w}_+ = \lambda_0\boldsymbol{w}_+ \tag{7}$$

and let $\boldsymbol{w}_-$, $\boldsymbol{v}_-$ be the left and right eigenvectors associated to the eigenvalue $-\lambda_0$. A straightforward calculation leads to the following relations:

$$\boldsymbol{v}_- = \boldsymbol{J}\boldsymbol{w}_+, \quad \boldsymbol{v}_+ = \boldsymbol{J}\boldsymbol{w}_-\,. \tag{8}$$

In particular, when $\lambda_0 = j\omega_0$ is an imaginary eigenvalue, we have $-\lambda_0 = -j\omega_0 = \lambda_0^*$. Consequently, we have $\boldsymbol{v}_- = (\boldsymbol{v}_+)^*$ and $\boldsymbol{w}_- = (\boldsymbol{w}_+)^*$ so that

$$\boldsymbol{w}_+ = -\boldsymbol{J}(\boldsymbol{v}_+)^* \quad \boldsymbol{w}_- = -\boldsymbol{J}(\boldsymbol{v}_-)^*\,. \tag{9}$$

These relations indicate that the left eigenvectors associated to imaginary eigenvalues do not need to be explicitly computed if the right eigenvectors are known. We will use this fact repeatedly.

C. Perturbation of Eigenvalues

Some basic results of the perturbation theory on eigenvalues [23] will be used for the passivity test and the passivity compensation algorithms. We consider a small perturbation of a generic matrix $\boldsymbol{Z}_0$, which we write as

$$\boldsymbol{Z}_\varepsilon = \boldsymbol{Z}_0 + \varepsilon\boldsymbol{Z}_1, \quad \varepsilon\to 0\,. \tag{10}$$

If we denote with λ_0 a simple eigenvalue of $\boldsymbol{Z}_0$ and with λ_ε its induced perturbation, for sufficiently small ε, there exists the convergent power series representation

$$\lambda_\varepsilon = \lambda_0 + k'\varepsilon + k''\varepsilon^2 + \cdots . \tag{11}$$

The first-order term can be characterized as

$$k' = \frac{\boldsymbol{w}^T \boldsymbol{Z}_1 \boldsymbol{v}}{\boldsymbol{w}^T \boldsymbol{v}} \tag{12}$$

where $\boldsymbol{w}, \boldsymbol{v}$ are the left and right eigenvectors of the unperturbed matrix $\boldsymbol{Z}_0$ associated to λ_0, normalized with unitary norm, i.e., $\|\boldsymbol{w}\| = \|\boldsymbol{v}\| = 1$. This result is also applicable if the multiplicity of λ_0 is larger than one, provided that there exists a complete set of eigenvectors for the associated eigenspace [23].

D. State–Space Multiport Representations

We consider a linear time-invariant multiport system $\mathcal{M}$ in state–space form

$$\mathcal{M}: \begin{cases} \dot{\boldsymbol{x}}(t) &= \boldsymbol{A}\boldsymbol{x}(t) + \boldsymbol{B}\boldsymbol{u}(t) \\ \boldsymbol{y}(t) &= \boldsymbol{C}\boldsymbol{x}(t) + \boldsymbol{D}\boldsymbol{u}(t) \end{cases} \tag{13}$$

where the dot denotes time differentiation. The number of ports and the dynamic order will be denoted by p and n, respectively, so that the state vector $\boldsymbol{x} \in \mathbb{R}^n$, input and output vectors $\boldsymbol{u}, \boldsymbol{y} \in \mathbb{R}^p$, and consequently, $\boldsymbol{A} \in \mathbb{R}^{n\times n}$, $\boldsymbol{B} \in \mathbb{R}^{n\times p}$, $\boldsymbol{C} \in \mathbb{R}^{p\times n}$, $\boldsymbol{D} \in \mathbb{R}^{p\times p}$. Two main multiport representations will be discussed, namely the scattering and the hybrid representation, the latter including as special cases both impedance (open-circuit) and admittance (short-circuit) representations. The input-output transfer matrix associated to (13) is

$$\boldsymbol{H}(s) = \boldsymbol{D} + \boldsymbol{C}(s\boldsymbol{I} - \boldsymbol{A})^{-1}\boldsymbol{B} \tag{14}$$

where s is the Laplace variable. Throughout the following we will assume that the system (13) is strictly stable, so that all eigenvalues of $\boldsymbol{A}$, or equivalently the poles of $\boldsymbol{H}(s)$ have a strictly negative real part. In addition, we will postulate both controllability and observability [14] for the state-space realization (13), which is thus assumed to be minimal. If this is not the case, standard reduction techniques can be applied. Finally, no assumptions on reciprocity will be made.

E. Passivity

A multiport is passive if it cannot generate energy. This is a key fact since the interconnection of passive multiports is guaranteed to be stable. On the other hand, stable but nonpassive systems may become unstable depending on the termination networks. This important fact is indeed what motivates this work. The precise definition of passivity for a multiport described by its transfer matrix (14) depends on the type of representation being adopted. For the particular case of hybrid representations, the transfer matrix must be positive real [2]. Since we consider only the case of strictly stable systems with no poles in the imaginary axis, the passivity condition may be expressed by requiring that the Hermitian part of the transfer matrix must be nonnegative definite on the imaginary axis, i.e.,

$$\boldsymbol{G}(j\omega) = \frac{1}{2}\left(\boldsymbol{H}(j\omega) + \boldsymbol{H}^H(j\omega)\right) \geq 0 \qquad \forall\omega\,. \tag{15}$$

This condition can be checked by ensuring that all its eigenvalues are nonnegative at any frequency

$$\lambda_i(j\omega) \geq 0 \qquad \forall\lambda_i(j\omega) \in \lambda(\boldsymbol{G}(j\omega)) \qquad \forall\omega\,. \tag{16}$$

Instead, in case of scattering representation, the transfer matrix must be unitary bounded, i.e.,

$$\left(\boldsymbol{I} - \boldsymbol{H}^H(j\omega)\boldsymbol{H}(j\omega)\right) \geq 0 \qquad \forall\omega\,. \tag{17}$$

This condition is equivalent to

$$\max_{i,\omega} \sigma_i(j\omega) \leq 1 \qquad \forall\sigma_i(j\omega) \in \sigma(\boldsymbol{H}(j\omega)) \tag{18}$$

which states that all singular values must be bounded by one at all frequencies. We have *strict passivity* if (16) or (18) are satisfied with strict inequalities. We remark that the conditions (16) and (18) can be easily checked at a set of individual discrete frequencies $\{\omega_k\}$. However, this frequency-sweep test for passivity may lead to erroneous results if the sampling is not accurate. This is the reason why purely algebraic passivity tests are regarded as more reliable. Tests based on the spectral properties of associated Hamiltonian matrices follow in this latter class, as detailed in Section III.

We will denote as *locally passive* for $\omega \in (\omega_a, \omega_b)$ a multiport satisfying conditions (15) and (17) only within the indicated frequency band. Similarly, an asymptotically passive system satisfies the passivity conditions for $s \to \infty$. In this work, we will assume a slightly stronger condition, namely *strict asymptotic passivity*. In the hybrid case such a condition reads

$$\min\left\{\lambda\left(\frac{(\boldsymbol{D} + \boldsymbol{D}^T)}{2}\right)\right\} = \lim_{\omega\to\infty} \min\{\lambda(\boldsymbol{G}(j\omega))\} > 0\,. \tag{19}$$

whereas in the scattering case, we have

$$\max\{\sigma(\boldsymbol{D})\} = \lim_{\omega\to\infty} \max\{\sigma(\boldsymbol{H}(j\omega))\} < 1\,. \tag{20}$$

Since both eigenvalues and singular values are continuous functions of frequency, these conditions insure that there exists an upper frequency $\omega_{\max} < \infty$ such that the system is strictly passive for $\omega \in (\omega_{\max}, \infty)$.

III. Characterization of Passivity Violations

The passivity of a multiport described by its transfer matrix (14) can be characterized at various levels of detail. One may be interested in a binary test answering the simple question whether the multiport is passive or not. However, more refined characterizations are possible. In particular, we will describe here an algebraic procedure that allows to pinpoint very accurately the frequency bands where passivity violations occur, i.e., where either (16) or (18), according to the specific representation being investigated, are not satisfied.

We begin this section by reporting the main results of [3]. These results will be the starting point for the further developments. The following two theorems motivate the introduction of Hamiltonian matrices for passivity characterization.

Theorem 1: (Scattering representation). Assume that $\boldsymbol{A}$ has no imaginary eigenvalues, $\gamma > 0$ is not a singular value of $\boldsymbol{D}$,

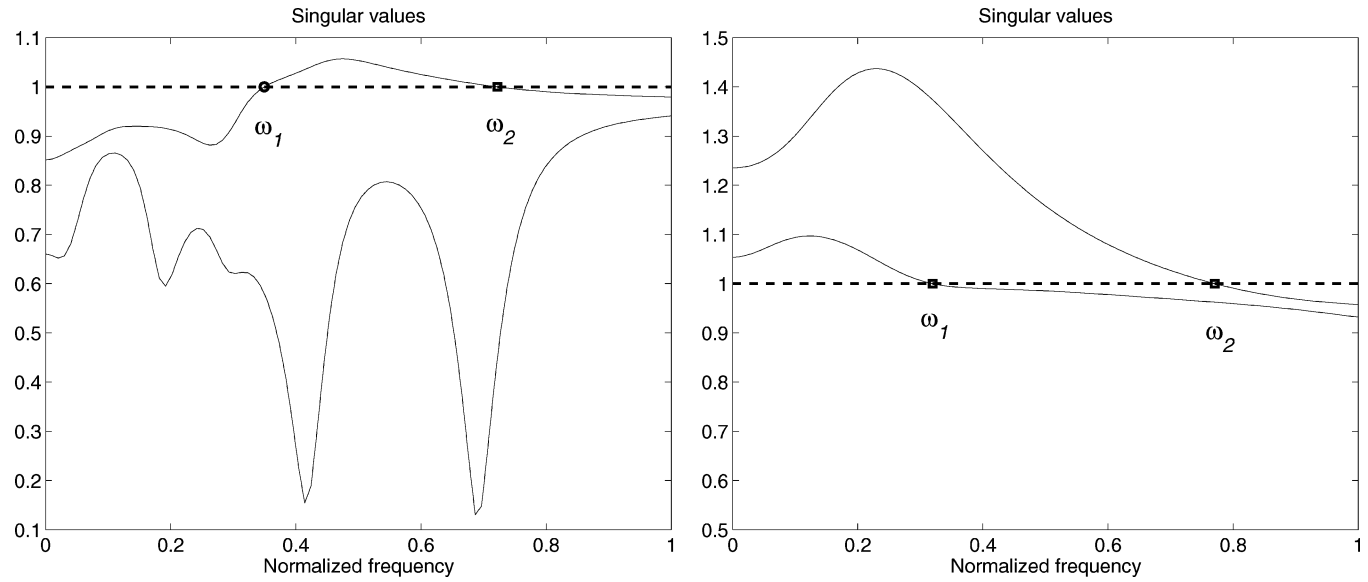

Fig. 1. Singular values distribution plotted versus normalized frequency for two different stable and nonpassive multiports.

and $\omega_0 \in \mathbb{R}$. Then, $\gamma \in \sigma(\boldsymbol{H}(j\omega_0))$ if and only if $j\omega_0 \in \lambda(\boldsymbol{M}_\gamma)$, where

$$\boldsymbol{M}_\gamma = \begin{pmatrix} \boldsymbol{A} - \boldsymbol{B}\boldsymbol{R}^{-1}\boldsymbol{D}^T\boldsymbol{C} & -\gamma\boldsymbol{B}\boldsymbol{R}^{-1}\boldsymbol{B}^T \\ \gamma\boldsymbol{C}^T\boldsymbol{S}^{-1}\boldsymbol{C} & -\boldsymbol{A}^T + \boldsymbol{C}^T\boldsymbol{D}\boldsymbol{R}^{-1}\boldsymbol{B}^T \end{pmatrix} \quad (21)$$

and $\boldsymbol{R} = (\boldsymbol{D}^T\boldsymbol{D} - \gamma^2\boldsymbol{I})$ and $\boldsymbol{S} = (\boldsymbol{D}\boldsymbol{D}^T - \gamma^2\boldsymbol{I})$.

The proof of this theorem, reported in [3], is based on a direct computation of the singular values of the transfer matrix and leads to the definition of $\boldsymbol{M}_\gamma$. A straightforward calculation shows that $\boldsymbol{M}_\gamma$ is a Hamiltonian matrix. Note that this theorem allows to compute the exact frequencies (if any) at which the singular values cross or touch any given threshold $\gamma = \gamma_0$. These frequencies are the imaginary eigenvalues of $\boldsymbol{M}_{\gamma_0}$. Therefore, setting this threshold to the maximum allowed value for passivity, i.e., $\gamma_0 = 1$, allows to derive a simple algebraic procedure for passivity test in case of scattering representation. However, some care must be taken in the design of this test, as discussed in the following. We state first the equivalent results for the hybrid representations.

Theorem 2: (Hybrid representations). Assume $\boldsymbol{A}$ has no imaginary eigenvalues, $\delta > 0$ is not an eigenvalue of $(\boldsymbol{D} + \boldsymbol{D}^T)/2$, and $\omega_0 \in \mathbb{R}$. Then, $\delta \in \lambda(\boldsymbol{G}(j\omega_0))$ if and only if $j\omega_0 \in \lambda(\boldsymbol{N}_\delta)$, where

$$\boldsymbol{N}_\delta = \begin{pmatrix} \boldsymbol{A} + \boldsymbol{B}\boldsymbol{Q}^{-1}\boldsymbol{C} & \boldsymbol{B}\boldsymbol{Q}^{-1}\boldsymbol{B}^T \\ -\boldsymbol{C}^T\boldsymbol{Q}^{-1}\boldsymbol{C} & -\boldsymbol{A}^T - \boldsymbol{C}^T\boldsymbol{Q}^{-1}\boldsymbol{B}^T \end{pmatrix} \quad (22)$$

and $\boldsymbol{Q} = (2\delta\boldsymbol{I} - \boldsymbol{D} - \boldsymbol{D}^T)$.

As for Theorem 1, Theorem 2 allows to compute the frequencies at which the eigenvalues of the Hermitian part of the transfer function cross or touch any given threshold $\delta = \delta_0$. A passivity test can be readily designed by using the critical level $\delta_0 = 0$. Since all multiport representations lead to investigate the spectral properties of associated Hamiltonian matrices, we will focus our attention on the scattering representation for the derivation of our results. The corresponding results for the hybrid case will only be summarized.

Let us consider the situation depicted in Fig. 1. Both panels show the frequency dependence of all singular values for two different stable and nonpassive two-ports ($n = 10$). The number of imaginary eigenvalues (with positive imaginary part) of the associated Hamiltonian matrix $\boldsymbol{M}_1$ is the same (two) for the two cases. The frequency axis is therefore subdivided into three frequency bands $(0, \omega_1)$, (ω_1, ω_2), and (ω_2, ∞). It is clear from this example that only the number of imaginary eigenvalues does not allow the local characterization of passivity in each frequency band. For example, the multiport depicted in the left panel is locally passive in $(0, \omega_1)$, while the one in the right panel is not. In fact, Theorem 1 does not give information on the number of singular values exceeding the threshold. Nonetheless, this type of information is very valuable when a passivity compensation algorithm is to be designed and applied.

A more careful look at Fig. 1 reveals that the situation in the two panels can be differentiated by the slope of singular values curves at the crossing points. The panel on the left has one crossing with positive slope at ω_1 and one with negative slope at ω_2. Conversely, the panel on the right has two crossings with negative slope at both frequencies. Since the singular values are continuous functions of frequency, the number of successive crossings with positive (negative) slopes can be precisely related to the number of singular values exceeding the threshold in each frequency band. These observations are made more precise in the following.

Let us consider the set of all imaginary eigenvalues (with positive imaginary part) of the Hamiltonian matrix at the critical level $\gamma = 1$, defined as

$$\Omega = \{\omega_i > 0 : j\omega_i \in \lambda(\boldsymbol{M}_1)\} \ . \quad (23)$$

We require that the multiplicity of each eigenvalue $j\omega_i$ is unitary for the moment. Generalizations will be discussed at the end of this section. Since the imaginary eigenvalues are simple, there exists a small disk surrounding $j\omega_i$ in the complex plane where no other eigenvalues are present. This allows to consider the perturbation of each eigenvalue in Ω induced by small variations

of the threshold γ around the critical level. More precisely, if we indicate with $\lambda_i^{(\gamma)} \in \lambda(\boldsymbol{M}_\gamma)$ the perturbation of the original eigenvalue $j\omega_i$ for $\gamma \simeq 1$, we have the following convergent power series representation:

$$\lambda_i^{(\gamma)} = j\omega_i + k_i'(\gamma - 1) + k_i''(\gamma - 1)^2 + \cdots . \tag{24}$$

The first-order coefficient k_i' is related to the slope of the singular value curve at the crossing, since

$$k_i' = \left.\frac{\mathrm{d}\lambda_i^{(\gamma)}}{\mathrm{d}\gamma}\right|_{\gamma=1} . \tag{25}$$

Note that k_i' is complex, so there is no guarantee in general that the perturbed eigenvalue will remain purely imaginary. However, we will show below that its real part vanishes in case of Hamiltonian matrices, so that the first-order perturbation can be written as

$$\lambda_i^{(\gamma)} = j\omega_i(\gamma) \simeq j\omega_i + j\Im\{k_i'\}(\gamma - 1) + \cdots . \tag{26}$$

This first-order coefficient can be computed using the perturbation theory results listed in Section II. We need to express the Hamiltonian matrix $\boldsymbol{M}_\gamma$ as a first-order expansion around the critical level. A straightforward calculation leads to the following expression:

$$\boldsymbol{M}_\gamma = \boldsymbol{M}_1 + (\gamma - 1)\boldsymbol{M'}_1 + \cdots \tag{27}$$

where

$$\boldsymbol{M'}_1 = \begin{pmatrix} -2\,\boldsymbol{B}\boldsymbol{R}_1^{-2}\boldsymbol{D}^T\boldsymbol{C} & -\boldsymbol{B}(2\boldsymbol{R}_1^{-2} + \boldsymbol{R}_1^{-1})\boldsymbol{B}^T \\ \boldsymbol{C}^T(2\boldsymbol{S}_1^{-2} + \boldsymbol{S}_1^{-1})\boldsymbol{C} & 2\,\boldsymbol{C}^T\boldsymbol{D}\boldsymbol{R}_1^{-2}\boldsymbol{B}^T \end{pmatrix} \tag{28}$$

where $\boldsymbol{R}_1 = (\boldsymbol{D}^T\boldsymbol{D} - \boldsymbol{I})$ and $\boldsymbol{S}_1 = (\boldsymbol{D}\boldsymbol{D}^T - \boldsymbol{I})$. Consequently, the expression of the first-order perturbation term on the imaginary eigenvalues reads, using (12)

$$k_i' = \frac{\boldsymbol{w}_i^T\boldsymbol{M'}_1\boldsymbol{v}_i}{\boldsymbol{w}_i^T\boldsymbol{v}_i} \tag{29}$$

where $\boldsymbol{w}_i, \boldsymbol{v}_i$ are the left and right eigenvectors associated to $j\omega_i$. This expression can be further simplified since the first-order expansion matrix $\boldsymbol{M'}_1$ is also a Hamiltonian matrix. Therefore, using (9), we have

$$k_i' = \frac{\boldsymbol{v}_i^H\boldsymbol{J}\boldsymbol{M'}_1\boldsymbol{v}_i}{\boldsymbol{v}_i^H\boldsymbol{J}\boldsymbol{v}_i} . \tag{30}$$

The denominator in this expression is purely imaginary since the matrix $\boldsymbol{J}$ is real and skew symmetric. Conversely, the matrix $\boldsymbol{J}\boldsymbol{M'}_1$ is real and symmetric, so the numerator is real. This confirms that the first-order perturbation of simple imaginary eigenvalues remains on the imaginary axis since $\Re\{k_i'\} = 0$. With reference to the examples depicted in Fig. 1, the real number

$$\xi_i = \frac{1}{\Im\{k_i'\}} = \frac{j\,\boldsymbol{v}_i^H\boldsymbol{J}\boldsymbol{v}_i}{\boldsymbol{v}_i^H\boldsymbol{J}\boldsymbol{M'}_1\boldsymbol{v}_i} \tag{31}$$

corresponds to the slope of the singular values versus frequency plots at the crossing points of the critical level $\gamma = 1$. These observations can be summarized by the following theorem, which gives a condition for the characterization of local passivity in the frequency bands determined by the breakpoints in the set Ω.

Theorem 3: (Scattering representation) Let Ω, defined as in (23), collect the (positive imaginary parts of the) imaginary eigenvalues of the Hamiltonian matrix $\boldsymbol{M}_\gamma$ in (21) at the critical level $\gamma = 1$, sorted in ascending order. Let all these imaginary eigenvalues be simple. Finally, let ξ_i be defined as in (31). Then, $\boldsymbol{H}(j\omega)$ is locally passive for $\omega \in (\omega_{i-1}, \omega_i)$ if and only if

$$\Lambda_i = \sum_{k \geq i} \mathrm{sgn}(\xi_k) = 0 \tag{32}$$

where $\mathrm{sgn}(\cdot)$ extracts the sign of its argument and $\omega_0 = 0$.

Proof: The proof follows immediately from the above considerations if the system is asymptotically passive. In fact, starting from the largest element in Ω and moving toward decreasing frequencies, each time a crossing (i.e., an element of Ω) is found with a negative slope, the number of singular values exceeding the critical level increases by one. Conversely, when a crossing is found with negative slope, this number decreases by one. Therefore, the sum in (32) indicates exactly the number of singular values exceeding the critical level in the frequency band (ω_{i-1}, ω_i). If this number equals zero, the system is locally passive in (ω_{i-1}, ω_i). □

We give now the corresponding result for the case of hybrid representations. The passivity characterization is summarized in the following theorem, that we state without proof.

Theorem 4: (Hybrid representation) Let Ω, defined as in (23), collect the (positive imaginary parts of the) imaginary eigenvalues of the Hamiltonian matrix $\boldsymbol{N}_\delta$ in (22) at the critical level $\delta = 0$, sorted in ascending order. Let all these imaginary eigenvalues be simple. Finally, let ζ_i be defined as

$$\zeta_i = \frac{j\,\boldsymbol{v}_i^H\boldsymbol{J}\boldsymbol{v}_i}{\boldsymbol{v}_i^H\boldsymbol{J}\boldsymbol{N'}_0\boldsymbol{v}_i} \tag{33}$$

where

$$\boldsymbol{N'}_0 = \begin{pmatrix} -2\,\boldsymbol{B}\boldsymbol{Q}_0^{-2}\boldsymbol{C} & -2\,\boldsymbol{B}\boldsymbol{Q}_0^{-2}\boldsymbol{B}^T \\ 2\,\boldsymbol{C}^T\boldsymbol{Q}_0^{-2}\boldsymbol{C} & 2\,\boldsymbol{C}^T\boldsymbol{Q}_0^{-2}\boldsymbol{B}^T \end{pmatrix} \tag{34}$$

with $\boldsymbol{Q}_0 = -(\boldsymbol{D}^T + \boldsymbol{D})$, denotes the first-order perturbation of $\boldsymbol{N}_\delta$ according to

$$\boldsymbol{N}_\delta = \boldsymbol{N}_0 + \delta\boldsymbol{N'}_0 + \cdots . \tag{35}$$

Then, $\boldsymbol{H}(j\omega)$ is locally passive for $\omega \in (\omega_{i-1}, \omega_i)$ if and only if

$$\Lambda_i = \sum_{k \geq i} \mathrm{sgn}(\xi_k) = 0 \tag{36}$$

where $\omega_0 = 0$.

Note that in this case the number of eigenvalues exceeding (from below) the critical level increases (decreases) when the

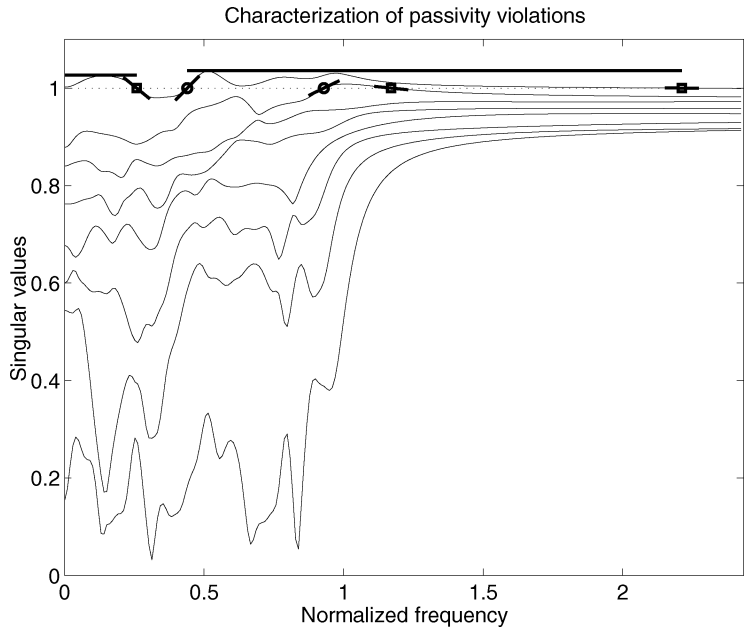

Fig. 2. Collective information gathered from the proposed passivity characterization algorithms. Breakpoints, slopes, and bounds for singular values are depicted with thick lines. The thin lines represent all singular values plotted versus frequency.

crossing has positive (negative) slope. This sign change does not affect the form of (36).

Theorems 3 and 4 provide a direct algebraic criterion for the characterization of passivity violation frequency bands. This criterion is summarized in the algorithm below for the scattering case. Obvious modifications apply for the hybrid representations.

Algorithm 1 *(Location of passivity violations).*
Compute the Hamiltonian matrix $\boldsymbol{M}_1$ *in* ***(21);***
Compute the imaginary eigenvalues of $\boldsymbol{M}_1$ and form the set Ω defined in **(23)**;
If Ω is empty,
 Multiport is passive, stop;
else
 Compute the matrix $\boldsymbol{M'}_1$ as in **(28)**;
 Compute the set of ξ_i as in **(31)**;
 For each element ω_i in the set Ω,
  Compute Λ_i according to **(32)**;
  if $\Lambda_i = 0$,
   multiport is locally passive in (ω_{i-1}, ω_i);
  else
   multiport is locally nonpassive in (ω_{i-1}, ω_i);
  end
 end
end.

The information provided by Algorithm 1 can be complemented by the quantification of the passivity violation in each frequency band. In particular, if (ω_{i-1}, ω_i) has been detected by Algorithm 1 to violate passivity, the bisection algorithm detailed in [3] can be used to determine the maximum value of the largest singular value within this band to any prescribed accuracy.

We illustrate the behavior of the proposed passivity characterization on a simple example. Fig. 2 shows the distribution of singular values for a synthetic stable and nonpassive multiport ($p = 8$ ports and $n = 41$ poles). The results of application of the proposed algorithms are superimposed with thick lines. Each frequency band where passivity violation occurs has been identified, and a corresponding estimate (with error bounds) for the maximum singular value has been generated. Note also that the slopes at the crossing points are indicated in the plot. This information will be used in Section IV for the design of a suitable algorithm for the compensation of these passivity violations.

A. Generalizations

The applicability of the passivity characterization procedure is general except for the requirement that the imaginary eigenvalues of the associated Hamiltonian matrices must be simple. In this section we discuss generalizations, analyzing the possible situations that may occur. We remark that the slopes defined in (31) and (33) are defined via first-order perturbations localized around a given imaginary eigenvalue $j\omega_i$. They are not influenced by the multiplicity of other eigenvalues distinct from $j\omega_i$. Consequently, we can focus on one eigenvalue at the time. Also, we discuss the case of scattering representation, obvious modifications applying in the hybrid case.

1) Nondefective Eigenspaces: A trivial generalization can be devised in presence of one imaginary eigenvalue $j\omega_i$ having multiplicity $\mu_i > 1$ and characterized by a complete set of (right) eigenvectors for the associated eigenspace. We denote these eigenvectors as

$$\{\boldsymbol{v}_{i,\nu}, \nu = 1, \ldots, \mu_i\}. \tag{37}$$

They form a basis of the eigenspace of dimension μ_i and lead to a purely diagonal block in the Jordan canonical form associated

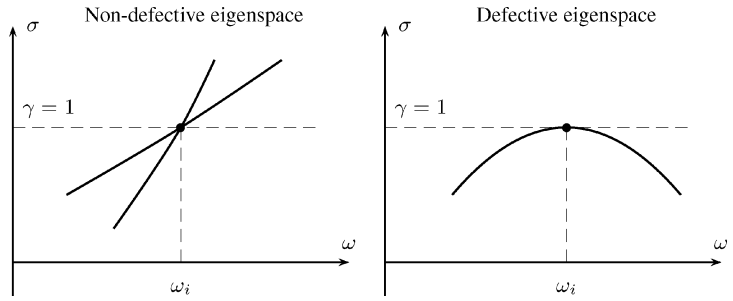

Fig. 3. Illustration of singular values behavior in case of a nonsimple imaginary eigenvalue $j\omega_i$ with multiplicity $\mu_i = 2$.

to the Hamiltonian matrix. For each of these eigenvectors we can compute the slopes as

$$\xi_{i,\nu} = \frac{j\, \boldsymbol{v}_{i,\nu}^H \boldsymbol{J}\boldsymbol{v}_{i,\nu}}{\boldsymbol{v}_{i,\nu}^H \boldsymbol{J}\boldsymbol{M}'_1 \boldsymbol{v}_{i,\nu}}, \qquad \nu = 1, \ldots, \mu_i\,. \tag{38}$$

It is clear that each of these slopes counts independently from the others in the computation of Λ_i as in (32). With obvious modifications Theorem 3 holds. We remark that this situation occurs when two separate singular values cross the critical level in the same frequency point, as illustrated in the left panel of Fig. 3.

2) Defective Eigenspaces: More care is to be taken in case of defective eigenspaces. In such case the number of independent eigenvectors is $\rho_i < \mu_i$, i.e., less than the multiplicity of the associated eigenvalue $j\omega_i$. The general situation may be very complex, so we discuss only the nonderogatory case, i.e., the case of only one eigenvector ($\rho = 1$), or equivalently, the case of a single Jordan block associated to the imaginary eigenvalue $j\omega_i$. In this case the theory developed in [23] shows that the μ_i perturbed eigenvalues $\{\lambda_{i,\nu},\ \nu = 1, \ldots, \mu_i\}$ are displaced by a dominant term which is not linear in the perturbation parameter $(\gamma - 1)$. More precisely, they are displaced within a small disk

$$|\lambda_{i,\nu} - j\omega_i| < \beta_i |\gamma - 1|^{1/\mu_i}, \qquad \nu = 1, \ldots, \mu_i \tag{39}$$

with some coefficient β_i. We illustrate the implications of this result in the simple case $\mu_i = 2$.

Let us consider the singular value behavior depicted in the right panel of Fig. 3, where a maximum occurs at the critical level $\gamma = 1$. We can write the quadratic expansion of the singular value curve around ω_i as

$$\sigma(\omega) \simeq 1 - a(\omega - \omega_i)^2, \qquad a > 0. \tag{40}$$

Inversion of this expression leads to

$$\omega - \omega_i \simeq \pm \sqrt{\frac{(1 - \sigma(\omega))}{a}} \tag{41}$$

which is compatible with the perturbation result of (39). In this situation, the singular value touches but does not cross the critical level $\gamma = 1$. Therefore, this eigenvalue should not be included in the evaluation of Λ_i in (32). This case can be generalized to any even multiplicity μ_i. Conversely, if the multiplicity is odd, the singular value curve will cross the critical level, and a more refined perturbation analysis is needed. For a discussion see [15]. In the most general derogatory case, i.e., with multiple Jordan blocks associated to the same eigenvalue $j\omega_i$, any combination of the above special cases may occur. It is clear that this general case requires a more careful analysis, which is beyond the scope of this work. We remark that in all our tests we have never encountered a case of defective Hamiltonian matrix, therefore Algorithm 1 could be applied without modifications.

IV. Passivity Enforcement

In this section, we address the problem of finding a passive approximation to a given stable but nonpassive multiport. In particular, we want to derive a new passive system $\mathcal{M}_p$ which is "close" in some sense to the original $\mathcal{M}$. Of course, this can be an ill-posed problem if the passivity violations are significant, since in such case any compensation of passivity may lead to a multiport with very different input-output behavior. Therefore, we give up any claim of generality, and we address the particular case of small passivity violations. This situation is nonetheless typical for the application area that motivates this paper, namely, macromodel generation for electrical interconnect structures. In a loose sense, we define as small passivity violations those requiring a small perturbation of the initial system in order to be compensated. This condition will be made more precise in the following.

Let us consider a state-space representation of the multiport $\mathcal{M}$ as in (13) and (14). The aim is to compute a new state-space realization $\mathcal{M}_p$ which satisfies the passivity requirements. We will impose the additional requirements listed below.

- The dynamic part of the original system will be preserved, in particular all the system poles will remain unchanged. This is guaranteed by preserving the state matrix $\boldsymbol{A}$ in the new system $\mathcal{M}_p$.
- The direct coupling at $s \to \infty$ should be preserved since we suppose that the original system $\mathcal{M}$ is asymptotically passive. Therefore, we will preserve also the state matrix $\boldsymbol{D}$.
- Since the transfer matrix of the system is linear in the state space matrices $\boldsymbol{B}$ and $\boldsymbol{C}$, it is convenient to apply a perturbation to only one of them and to leave the other unchanged. We will retain $\boldsymbol{B}$ and we will modify only matrix $\boldsymbol{C}$. The feasibility of this approach is guaranteed by the underlying hypotheses of controllability and observability.

As a result, we will consider the modified state-space system

$$\mathcal{M}_p : \begin{cases} \dot{\boldsymbol{x}}(t) &= \boldsymbol{A}\boldsymbol{x}(t) + \boldsymbol{B}\boldsymbol{u}(t) \\ \boldsymbol{y}(t) &= \boldsymbol{C}_p\boldsymbol{x}(t) + \boldsymbol{D}\boldsymbol{u}(t) \end{cases} \tag{42}$$

where only the matrix $\boldsymbol{C}$ is perturbed in order to satisfy passivity. We remark that this is not the only possible choice for the passivity compensation, but this will the only one herewith investigated.

A. Criteria for Best Approximation

First, we will derive suitable conditions on the perturbed matrix $\boldsymbol{C}_p$ that guarantee the minimal deviation of the input-output responses from those of the original system. Let

$$\boldsymbol{dC} = \boldsymbol{C}_p - \boldsymbol{C} \tag{43}$$

indicate the perturbation of the state matrix. We consider the difference in the impulse response matrices of the two systems induced by this perturbation, expressed as

$$\boldsymbol{dh}(t) = \mathcal{L}^{-1}\{\boldsymbol{dH}(s)\} = \boldsymbol{dC}\exp\{\boldsymbol{A}t\}\boldsymbol{B}\,, \qquad t \geq 0\,. \tag{44}$$

The new matrix $\boldsymbol{C}_p$ will be derived in order to minimize the following functional expressing the cumulative energy of the impulse responses perturbations

$$\begin{aligned} E &= \sum_{i,j=1}^{p} \int_0^\infty |(dh)_{i,j}(t)|^2 \,\mathrm{d}t = \int_0^\infty \|\boldsymbol{dh}(t)\|_F^2 \,\mathrm{d}t \\ &= \int_0^\infty \mathrm{tr}\left(\boldsymbol{dh}(t)\boldsymbol{dh}^T(t)\right) \,\mathrm{d}t\,. \end{aligned} \tag{45}$$

A straightforward substitution of (44) into the above expression leads to

$$E = \mathrm{tr}\left(\boldsymbol{dC}\,\boldsymbol{W}\,\boldsymbol{dC}^T\right) \tag{46}$$

where $\boldsymbol{W}$ is the controllability Gramian [5] defined as

$$\boldsymbol{W} = \int_0^\infty \exp\{\boldsymbol{A}t\}\boldsymbol{B}\boldsymbol{B}^T \exp\{\boldsymbol{A}^T t\}\,\mathrm{d}t\,. \tag{47}$$

This can be computed as the unique symmetric and positive definite solution of the Lyapunov equation

$$\boldsymbol{A}\boldsymbol{W} + \boldsymbol{W}\boldsymbol{A}^T = -\boldsymbol{B}\boldsymbol{B}^T\,. \tag{48}$$

Due to the controllability assumption the Gramian admits a Cholesky factorization

$$\boldsymbol{W} = \boldsymbol{K}^T\boldsymbol{K} \tag{49}$$

where $\boldsymbol{K}$ is a nonsingular upper triangular matrix. Therefore, we can express the perturbation of $\boldsymbol{dC}$ in a new coordinate system induced by a change of basis defined by the Cholesky factors,

$$\boldsymbol{dC_k} = \boldsymbol{dC}\,\boldsymbol{K}^T\,. \tag{50}$$

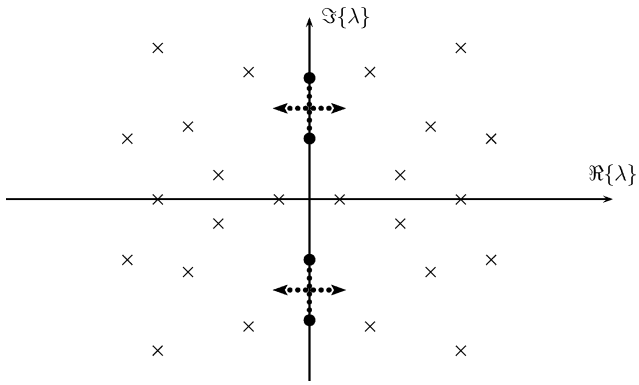

Fig. 4. Perturbation of imaginary eigenvalues of Hamiltonian matrix.

Substitution into (46) leads to

$$E = \mathrm{tr}\left(\boldsymbol{dC_k}\boldsymbol{dC_k}^T\right) = \|\boldsymbol{dC_k}\|_F^2 = \|\mathrm{vec}(\boldsymbol{dC_k})\|_2^2\,. \tag{51}$$

The latter expression shows that minimization of the impulse responses perturbations is achieved by minimizing the perturbation of the state matrix $\boldsymbol{C}$, using the appropriate coordinate system.

B. Passivity Compensation Algorithm

This section presents an iterative algorithm for the compensation of small passivity violations. We will assume that the Algorithm 1 has been applied to characterize all frequency intervals where passivity violations occur, and accurate estimates of the violation amounts (largest singular value or smallest eigenvalue according to the representation being adopted) are available [3]. As in Section III, we will focus on the scattering representation case for the presentation of the results, and we will summarize only the equivalent results for the hybrid representations.

The main algorithm is based on the spectral properties of the associated Hamiltonian matrix $\boldsymbol{M}_\gamma$ at the critical level $\gamma = 1$. We illustrate the main idea through a simple example. Let us assume that the characteristic polynomial of the Hamiltonian matrix can be written as

$$p(\lambda) = p_r(\lambda)p_i(\lambda), \quad p_i(\lambda) = \left[\left(\lambda^2 + \omega_0^2\right)^2 + \epsilon\right] \tag{52}$$

where $p_r(\lambda)$ has no roots in small disks surrounding $\pm j\omega_0$ and where $|\epsilon| \ll \omega_0$. With reference to Fig. 4, the roots of $p_r(\lambda)$ are depicted with crosses, while the roots of $p_i(\lambda)$ are depicted by dots. According to the sign of the small parameter ϵ, we may have the following three cases (using a first-order expansion in ϵ)

$$p_i(\lambda) = 0 \quad \Longleftrightarrow \quad \begin{cases} \lambda = \pm j(\omega_0 \pm \sqrt{-\epsilon\omega_0}), & \text{if } \epsilon < 0 \\ \lambda = \pm j\omega_0(\text{double}), & \text{if } \epsilon = 0 \\ \lambda \simeq \pm\sqrt{\epsilon\omega_0} \pm j\omega_0, & \text{if } \epsilon > 0. \end{cases} \tag{53}$$

with any possible combination of signs. This example shows that a small perturbation may be applied (see Fig. 4) in order to displace purely imaginary eigenvalues ($\epsilon < 0$) off the imaginary

axis ($\epsilon > 0$). Of course, the general case may be much more complicated than this simple situation. We will discuss in detail the various cases that may occur in the following paragraphs.

We will apply first-order perturbations on the matrix $\boldsymbol{M}_1$ in order to displace its imaginary eigenvalues and eventually force them to move off the imaginary axis. We will achieve this by computing the perturbation $\boldsymbol{dC}$ on the state matrix $\boldsymbol{C}$ as in (43) that is needed to move the eigenvalues in the correct direction. Note that the level γ is now kept fixed at the critical level $\gamma = 1$. From definition (21) we can write

$$\boldsymbol{M}_1|_p = \boldsymbol{M}_1 + \boldsymbol{dM}_1 \tag{54}$$

where the perturbation matrix $\boldsymbol{dM}_1$, neglecting the second-order terms, reads

$$\boldsymbol{dM}_1 \simeq \begin{pmatrix} -\boldsymbol{B}\boldsymbol{R}_1^{-1}\boldsymbol{D}^T\boldsymbol{dC} & \boldsymbol{0} \\ \boldsymbol{C}^T\boldsymbol{S}_1^{-1}\boldsymbol{dC} + \boldsymbol{dC}^T\boldsymbol{S}_1^{-1}\boldsymbol{C} & \boldsymbol{dC}^T\boldsymbol{D}\boldsymbol{R}_1^{-1}\boldsymbol{B}^T \end{pmatrix}. \tag{55}$$

A straightforward check shows that also $\boldsymbol{dM}_1$ is a Hamiltonian matrix. Therefore, the first-order perturbations induced on the imaginary eigenvalues of $\boldsymbol{M}_1$ remain imaginary if the perturbation term is sufficiently small. We want to design the perturbation, i.e., find the matrix $\boldsymbol{dC}$, in order to displace each imaginary eigenvalue $j\omega_i$ by a prescribed quantity. If the new location is denoted $j\omega_{i,p}$, we have the first-order approximation

$$j\omega_{i,p} - j\omega_i \simeq \frac{\boldsymbol{v}_i^H \boldsymbol{J}\boldsymbol{dM}_1\boldsymbol{v}_i}{\boldsymbol{v}_i^H \boldsymbol{J}\boldsymbol{v}_i}. \tag{56}$$

We now express the numerator as a linear expression of the perturbation $\boldsymbol{dC}$. To this end, it is convenient to partition the eigenvector $\boldsymbol{v}_i$ using the induced block partition of the Hamiltonian matrix, as $\boldsymbol{v}_i = (\boldsymbol{v}_{i1}^T, \boldsymbol{v}_{i2}^T)^T$. Simple algebraic manipulations lead to the expression

$$\boldsymbol{v}_i^H \boldsymbol{J}\boldsymbol{dM}_1\boldsymbol{v}_i = 2\,\Re\{\boldsymbol{z}_i^H \boldsymbol{dC}\,\boldsymbol{v}_{i1}\} \tag{57}$$

where

$$\boldsymbol{z}_i = \boldsymbol{D}\boldsymbol{R}_1^{-1}\boldsymbol{B}^T\boldsymbol{v}_{i2} + \boldsymbol{S}_1^{-1}\boldsymbol{C}\,\boldsymbol{v}_{i1}. \tag{58}$$

Now using the basis change in (50) and the property (3) of the Kronecker product we can write

$$\boldsymbol{v}_i^H \boldsymbol{J}\boldsymbol{dM}_1\boldsymbol{v}_i = 2\,\Re\{(\boldsymbol{v}_{i1}^T\boldsymbol{K}^{-1}) \otimes \boldsymbol{z}_i^H\}\,\mathrm{vec}(\boldsymbol{dC_k}). \tag{59}$$

In summary, the state matrix perturbation $\boldsymbol{dC_k}$ that is required for a small displacement of the imaginary eigenvalue $j\omega_i$ into the new location $j\omega_{i,p}$ must satisfy the condition

$$2\,\Re\{(\boldsymbol{v}_{i1}^T\boldsymbol{K}^{-1}) \otimes \boldsymbol{z}_i^H\}\,\mathrm{vec}(\boldsymbol{dC_k}) = -\Im\{\boldsymbol{v}_i^H \boldsymbol{J}\boldsymbol{v}_i\}\,(\omega_{i,p} - \omega_i). \tag{60}$$

This is a linear constraint, since it has been derived using first-order approximations. For each imaginary eigenvalue in the set Ω a constraint (60) can be devised once a suitable location for the perturbed eigenvalues has been defined. All these constraints can be collected in a compact matrix form

$$\boldsymbol{Z}\,\mathrm{vec}(\boldsymbol{dC_k}) = \boldsymbol{r}, \qquad \min \|\mathrm{vec}(\boldsymbol{dC_k})\|_2 \tag{61}$$

where also the best approximation condition that minimizes (51) has been included. Each row in matrix $\boldsymbol{Z}$ stores the left-hand side of (60). This is a standard least squares problem whose solution does not require special care. Note that this problem is usually underdetermined since the number of unknowns is $n \times p$, while the number of linear constraints matches the number of imaginary eigenvalues pairs, which is bounded by the dynamic order n. The condition on the right in (61) insures that the particular solution that minimizes the deviation from the input output behavior of the original system is actually computed.

We focus now on the determination of the new eigenvalue locations. We may refer to the example in Fig. 2 for illustration. We want to obtain the effect of lowering the singular values curves below the critical level $\gamma = 1$. It is clear that this effect can be achieved by moving each crossing point in the direction pointed by its slope, i.e., eigenvalues with positive slopes are moved toward higher frequencies, while eigenvalues with negative slopes are moved toward lower frequencies. Note that this would also be equivalent to raising the critical level of a small amount above one. The above observations give only information on the correct sign that should be used for the right-hand side in (60). The amount of displacement for each eigenvalue should be determined in order to satisfy the first-order assumptions. Several cases may apply, as itemized below.

- We consider first the simple case of a localized passivity violation with only one singular value exceeding the critical level. This situation is illustrated in the left panel of Fig. 5. The dashed lines represent the information collected using Algorithm 1 and the bisection algorithm in [3], i.e., local slopes ξ_i at the crossing points and an estimate for the local maximum $\sigma_{\max}$. A possible choice for the determination of the new locations is the intersection between the upper bound and the two tangent lines at the crossing points

$$(\omega_{i,p} - \omega_i) \equiv \xi_i^{-1}\,(\sigma_{\max} - 1). \tag{62}$$

- The case illustrated above is characterized by a uniformly concave behavior of the singular value curve throughout the violation interval. This may not always be the case, as illustrated in the middle panel of Fig. 5. In this case, the intersection with the upper bound $\sigma_{\max}$ as in (62) leads to no useful information, since it may be even outside the violation bandwidth. Therefore, as an additional constraint, we will set an upper bound on the eigenvalue displacement based on the distance between the two edges of the violation bandwidth $\Delta = \omega_i - \omega_{i-1}$. We set

$$\begin{cases} (\omega_{i,p} - \omega_i) \le \alpha(\omega_{i+1} - \omega_i), & \text{for } \xi_i > 0 \\ (\omega_i - \omega_{i,p}) \le \alpha(\omega_i - \omega_{i-1}), & \text{for } \xi_i < 0. \end{cases} \tag{63}$$

  The factor $0 < \alpha < 0.5$ can be used to tune the performance of the algorithm. Investigations on the influence of this parameter on the algorithm are presented in Section V.A.
- Another situation that may occur is the case of two adjacent crossing points having slopes with equal sign. Also in this case, illustrated in the right panel of Fig. 5, the intersection between tangent and upper bound provides no

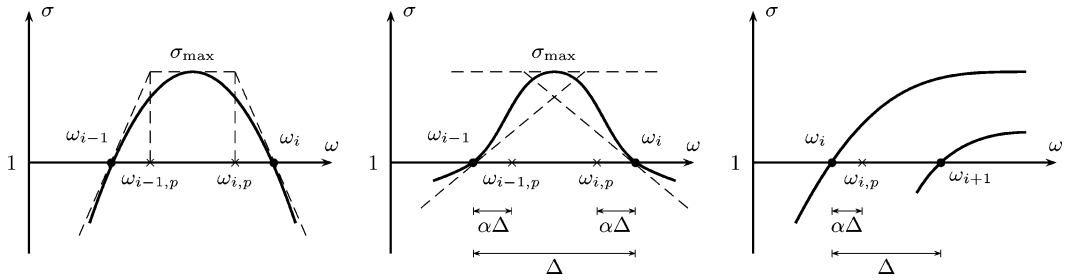

Fig. 5. Determination of the perturbed eigenvalue locations $\omega_{i,p}$ (crosses) for various possible situations. The dots denote the unperturbed eigenvalues. See text for details.

useful information. Therefore, we use an upper bound similar to (63) by restricting the displacement of each eigenvalue by an amount not larger than α times its distance from the nearest eigenvalue in the direction pointed by its slope.

The most general case may be any combination of these three scenarios, with possibly many singular values exceeding the critical level in some frequency intervals. Therefore, the procedure for the displacement of the eigenvalues must be iterated until all imaginary eigenvalues have been displaced. We have the following algorithm.

Algorithm 2 (Passivity enforcement).
Set $m = 0$ and $\boldsymbol{C}_0 = \boldsymbol{C}$;
Apply Algorithm 1 using $\boldsymbol{C}_0$ and form the set Ω;
Repeat
Increase the iteration count $m := m + 1$;
Apply the bisection algorithm in **[3]** to each violation bandwidth;
Determine the new eigenvalues locations $\omega_{i,p}$ using **(62)** and **(63)**;
Solve the linear least squares problem **(61)** and compute $\boldsymbol{dC}_m$ using **(50)**;
Update the state matrix $\boldsymbol{C}_m = \boldsymbol{C}_{m-1} + \boldsymbol{dC}_m$;
Apply Algorithm 1 using $\boldsymbol{C}_m$ and form the set Ω;
Until Ω is empty.

If the algorithm stops in q iterations, exactly q first-order perturbations to the state-space matrix $\boldsymbol{C}$ have been applied. In particular, the new state matrix $\boldsymbol{C}_q$ is expressed by

$$\boldsymbol{C}_q = \boldsymbol{C} + \sum_{m=1}^{q} \boldsymbol{dC}_m \,. \tag{64}$$

The hypothesis of initial small passivity violation can be verified on the relative perturbation that was necessary to compensate it, i.e., by checking the condition

$$\|\boldsymbol{C}_q - \boldsymbol{C}\|_F \ll \|\boldsymbol{C}\|_F \,. \tag{65}$$

This condition insures that the input-output responses of the modified passive system are close in a suitable norm (see Section IV.A) to those of the original nonpassive system. Condition (65) can be inserted as an additional check for stopping iterations in Algorithm 2 in order to detect whether the passivity violations in the original system are not sufficiently small to be compensated via first-order perturbations. We remark that, in principle, Algorithm 2 could be applied in case of large passivity violations, i.e., not satisfying (65). However, no tests were performed in such cases. We expect that, for large passivity violations, the number of required iterations may be large, and consequently other approaches should be attempted.

We summarize now the passivity compensation algorithm for the hybrid representation case. The perturbation on the Hamiltonian matrix $\boldsymbol{N}_\delta$ in (22) at the critical level $\delta = 0$ induced by small perturbations in the state matrix $\boldsymbol{C}$ reads

$$\boldsymbol{N}_0|_p = \boldsymbol{N}_0 + \boldsymbol{dN}_0 \tag{66}$$

where, neglecting the second-order terms

$$\boldsymbol{dN}_0 \simeq \begin{pmatrix} \boldsymbol{B}\boldsymbol{Q}_0^{-1}\boldsymbol{dC} & \boldsymbol{0} \\ -\boldsymbol{C}^T\boldsymbol{Q}_0^{-1}\boldsymbol{dC} - \boldsymbol{dC}^T\boldsymbol{Q}_0^{-1}\boldsymbol{C} & -\boldsymbol{dC}^T\boldsymbol{Q}_0^{-1}\boldsymbol{B}^T \end{pmatrix}. \tag{67}$$

Using this expression and repeating the above calculations, we are led to define, for each imaginary eigenvalue $j\omega_i$ of $\boldsymbol{N}_0$ the vector

$$z_i = -\boldsymbol{Q}_0^{-1}\boldsymbol{B}^T\boldsymbol{v}_{i2} - \boldsymbol{Q}_0^{-1}\boldsymbol{C}\boldsymbol{v}_{i1} \tag{68}$$

which replaces the corresponding definition in (58) relative to the scattering case. Using the above modifications we can write a set linear constraints in the form (60) and assemble them in a compact form as in (61). With these new definitions, Algorithm 2 can be applied for the passivity compensation also in case of hybrid representations.

C. Algorithm Complexity

This section provides a discussion on the computational complexity of the proposed passivity compensation algorithm and highlights possible future improvements. The most demanding parts of Algorithm 2 are

- Computation of imaginary eigenvalues of the Hamiltonian matrix. This general problem requires $O(n^3)$ operations.
- The above computation must be repeated at each iteration, thus making the computational compexity of the algorithm problem-dependent.
- The numerical solution of the Lyapunov (48) and the corresponding Cholesky factorization (49). This requires $O(n^3)$ as well, but this computation is performed only once before starting the iterations.
- The solution of the least-squares system (61). The computational cost for solving this system is $n_i^2 np - n_i^3/3$, where

n_i is the number of imaginary eigenvalues pairs to be perturbed. Since generally $n_i \leq n$ and usually $n_i \ll n$, this operation is less critical than the above listed ones.

The above discussion shows that the CPU time is dominated by the determination of the eigenvalues of the Hamiltonian matrix, which is therefore $O(n^3)$ per iteration. However, this applies if the standard Schur decomposition is blindly used for this computation. The present implementation of the algorithm is still lacking any optimization in this respect. However, the following points should be considered

- The stucture of any Hamiltonian matrix is very particular, and its spectrum is characterized by a high degree of symmetry. Therefore, there is a large margin for the development of a customized eigenvalue solver that fully exploits this structure.
- The particular type of macromodels being considered have a quite sparse state-space representation. In particular, $\boldsymbol{A}$ and $\boldsymbol{B}$ are nearly diagonal and block-diagonal. This sparsity is not currently exploited in the eigenvalue solver, which (at the moment) works only on full matrices.
- Only the imaginary eigenvalues are needed and not the full spectrum. Currently, all eigenvalues are found and the imaginary ones are extracted a posteriori.

Based on the above observations, we conclude that the current implementation of Algorithm 2 is immediately applicable to small and medium sized problems with high efficiency. Larger problems will need an optimized eigenvalue solver. Progress in this direction will be documented in a future report.

V. Numerical Examples

This section illustrates the performance of the passivity check and compensation algorithms. We will use in some cases synthetic multiports that have been generated ad hoc in order to illustrate special features of the algorithms. In other cases, some nonpassive macromodels arising from rational approximation algorithms will be analyzed.

A. Algorithm Parameterization

This section illustrates the influence of the parameter α introduced in (63) on the performance of the algorithm for passivity enforcement. We recall that this parameter is used to limit the displacement of each eigenvalue with respect to its distance to its closest neighbor. We will consider the simple one-port test problem characterized by the following state matrices (scattering representation)

$$\boldsymbol{A} = \begin{pmatrix} -\frac{1}{2} & 1 \\ -1 & -\frac{1}{2} \end{pmatrix} \quad \boldsymbol{B} = \boldsymbol{C}^T = \begin{pmatrix} \frac{1}{2} \\ \frac{1}{2} \end{pmatrix} \quad \boldsymbol{D} = \frac{1}{2}. \tag{69}$$

A simple substitution into (21) leads to the following associated Hamiltonian matrix

$$\boldsymbol{M}_1 = \frac{1}{6} \begin{pmatrix} -2 & 7 & 2 & 2 \\ -5 & -2 & 2 & 2 \\ -2 & -2 & 2 & 5 \\ -2 & -2 & -7 & 2 \end{pmatrix} \tag{70}$$

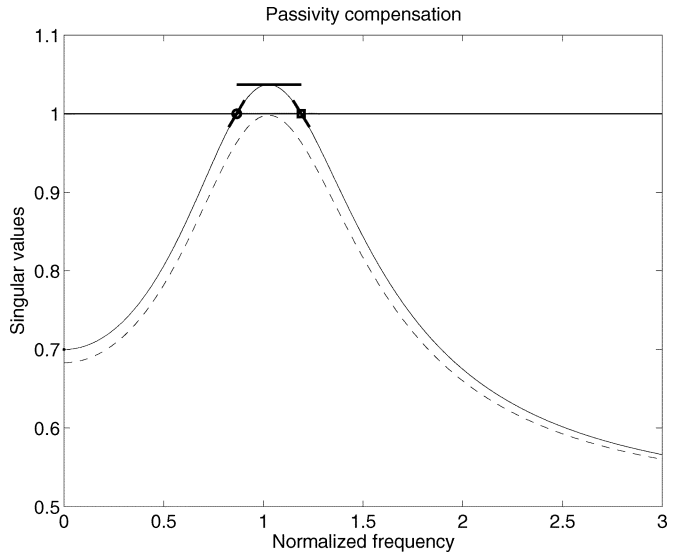

Fig. 6. Singular value plot (solid line) for the test system (69) and for the compensated system obtained using $\alpha = 0.3$ (dashed line). Only one iteration is required for the passivity compensation.

TABLE I
Influence of Parameter α on Performance of Passivity Enforcement Algorithm

α	Iterations	$\|\|d\boldsymbol{C}\|\|/\|\|\boldsymbol{C}\|\|$
0.1	43	0.0661
0.2	13	0.0661
0.25	4	0.0661
0.255	2	0.0661
0.26	1	0.0670
0.27	1	0.0691
0.28	1	0.0704
0.3	1	0.0704
0.4	1	0.0704

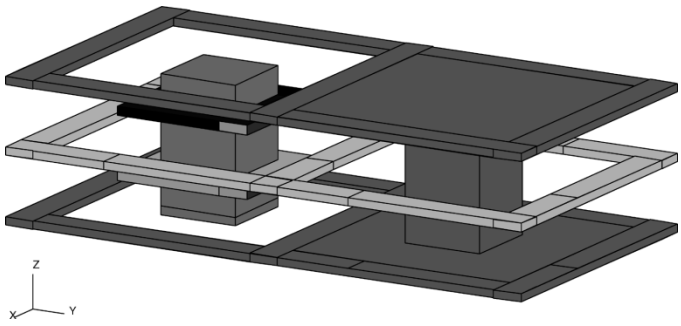

Fig. 7. Single via structure. Two ports are defined between vertical conductor and top (bottom) ground planes.

whose four eigenvalues are purely imaginary. Precisely, the set Ω of (23) reads

$$\Omega = \{0.866,\ 1.190\} \tag{71}$$

whereas the maximum value of the (unique) singular value is $\sigma_{\max} = 1.037$. The frequency behavior of the singular value is depicted in Fig. 6. The passivity compensation algorithm has been run using several different values of the control parameter α. The results are summarized in Table I.

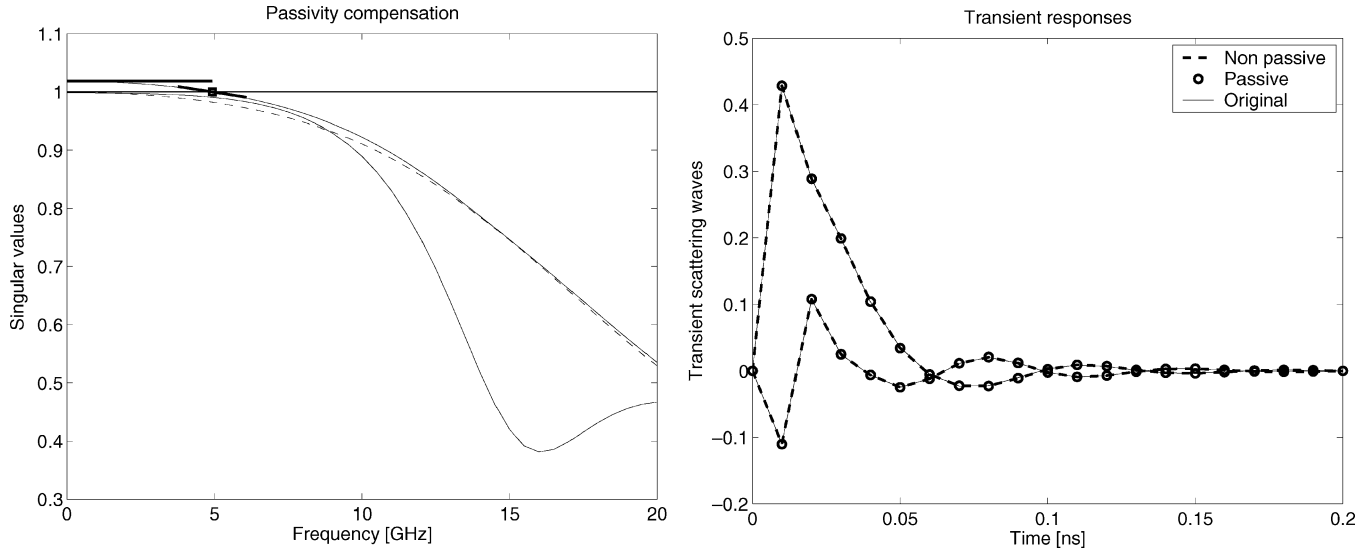

Fig. 8. Passivity compensation for the single via structure of Fig. 7. Left panel: singular values for the nonpassive macromodel (thin solid lines) and for the passive macromodel (thin dashed lines). Right panel: transient responses.

The results in the table are easily justified as follows. With reference to the illustrations in the left panel of Fig. 5, the intersection between the tangents at the crossing points and the upper bound computed via (62) leads to a displacement of the two eigenvalues by a fraction of 0.275 and 0.262 of the entire violation bandwidth, respectively. Therefore, for values of α larger than 0.275 this parameter has no effect. The table shows that, in this case, only one iteration is sufficient for the compensation of passivity. Conversely, smaller values of α limit the displacement of the perturbed eigenvalues and provide a better guarantee of validity for the first-order approximations used in the algorithm. However, if smaller perturbations are applied, a larger number of iterations are necessary to reach passivity. It is clear that when α is too small the algorithm becomes very inefficient (43 iterations if $\alpha = 0.1$), although it provides passivity compensation using smaller and more accurate perturbations on the original system. The data on relative perturbation applied to the state matrix $\boldsymbol{C}$ in order to reach passivity clearly indicate that use of a very small value for α is not justified. We have performed extensive testing on various systems with varying number of ports and dynamic order. A value of $\alpha = 0.3$ seems to be a reasonable compromise, so this value is used for all numerical examples reported in this work.

B. Macromodeling of Electrical Interconnects

This section presents a few application examples to electrical modeling of three-dimensional interconnects. We will concentrate on the issue of passivity check and compensation of lumped macromodels, and we will not give extensive details on how the macromodels have been generated. However, a small summary of the various modeling steps is presented for each case.

1) Single via Structure: The first structure that will be investigated is a two-port ($p = 2$) macromodel derived for a single via interconnect crossing a solid metal plane. The structure is depicted in Fig. 7. The two ports are defined between the vertical

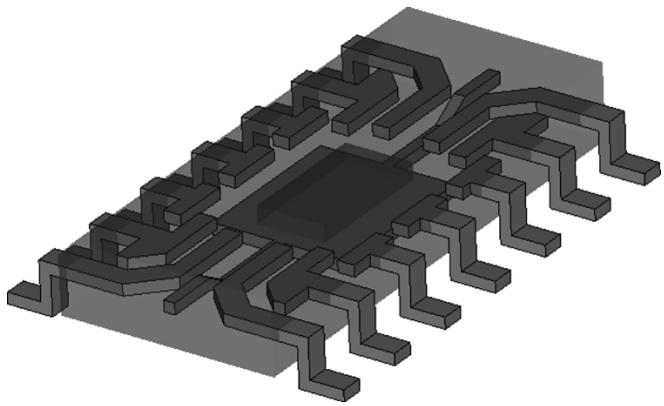

Fig. 9. Surface mount package structure with 14 pins (28 ports). Bonding wires and printed circuit board on which package is mounted are not shown.

conductor and top and bottom planes, respectively. The structure has been meshed and analyzed via the partial element equivalent circuit (PEEC) method (see, e.g., [18] and references therein). A time-domain full-wave formulation has been adopted, including retardation to take into account propagation effects. The PEEC scheme has been solved in time-domain to obtain the scattering port responses (referenced to 50-Ω loads) to a unitary triangle pulse excitation with a 10 ps rise and fall time. These responses have been processed by a time-domain vector fitting algorithm [10], [11], and a rational approximation to the transfer matrix has been derived. The resulting number of poles is $n_p = 5$. Finally, a state-space realization in Jordan canonical form has been obtained using the procedure of [1], with a size of the state matrix $\boldsymbol{A}$ of $n = 10$ (all residue matrices of the approximation have full rank, therefore $n = p \times n_p$). The resulting state-space realization is nonpassive, as shown in Fig. 8. Note that the passivity violation is in a localized frequency band in the low frequency range. This passivity violation has been characterized via Algorithm 1 and the bisection algorithm in [3], obtaining the slope at the (unique) crossing point and the upper bound for

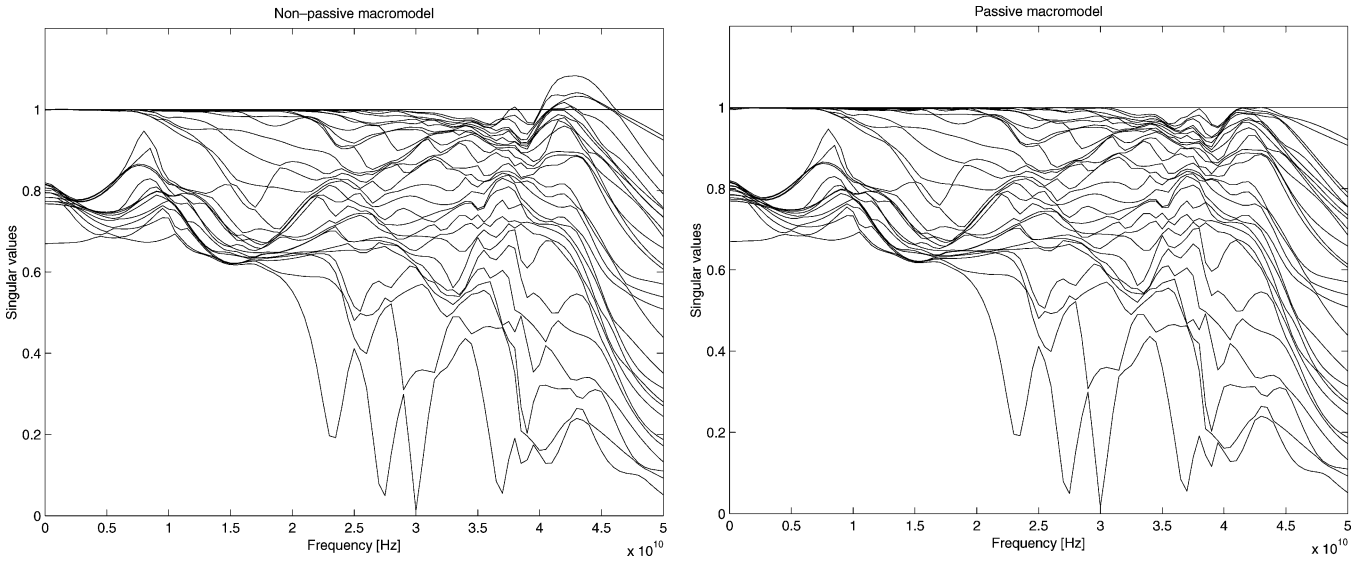

Fig. 10. Passivity compensation for the package structure of Fig. 9. The singular values are plotted versus frequency for the nonpassive macromodel (left panel) and for the passive macromodel (right panel).

the singular values in the violation interval. Finally, Algorithm 2 has been applied to compensate the passivity violation. Only one iteration was necessary for compensation, requiring a fraction of a second of CPU time on a 2-GHz Pentium IV-based notebook. The singular values of the passive macromodel are shown for comparison in the left panel of Fig. 8. The three sets of transient responses (original, nonpassive macromodel, passive macromodel) are depicted in the right panel of Fig. 8. A very good accuracy has been achieved in the reproduction of the input-output behavior of the via structure in a broad range of frequencies. Note that the perturbation $\boldsymbol{dC}$ that was necessary for passivity compensation is such that

$$\|\boldsymbol{dC}\|_F = 0.036\,\|\boldsymbol{C}\|_F \tag{72}$$

which confirms that the passivity violation in the raw macromodel was actually small.

2) Package Structure: The last example that we consider is a commercial 14-pin surface mount package depicted in Fig. 9. The structure has $p = 28$ ports, half being defined between a corresponding pin and the printed circuit board on which the package is mounted, and half being defined between the bonding pad on the included die and the reference plane below the die itself. All ports are defined using a 50-Ω reference load. The structure has been meshed and analyzed with a full-wave electromagnetic solver based on the finite-difference time-domain (FDTD) method [21]. The raw dataset obtained by FDTD is a set of 28×28 transient scattering responses due to Gaussian pulse excitation having a 30 GHz frequency bandwidth. Note that an extended bandwidth was used for macromodel generation, in order to stress the robustness of the algorithms. Indeed, at these frequencies, propagation delays and distributed couplings make the macromodeling task quite challenging.

The complete set of responses has been processed by a time-domain vector fitting algorithm [10], [11] in order to derive a fully coupled rational macromodel. Two different procedures were applied. The first used a common set of 30 poles for all the transfer matrix entries. However, all the corresponding matrices of residues in the partial fraction expansion of the transfer matrix had a full numerical rank, leading to a state-space realization of order $28 \times 30 = 840$. The second approach used a private set of 30 poles for each column of the transfer matrix. The resulting order of the state space realization was the same, but the accuracy was significantly better. Results are presented for this latter macromodel. Passivity was characterized using the algorithms presented in this paper. The singular values distribution is depicted in the left panel of Fig. 10 (the crossing points and the slopes are not shown for clarity). A total number of 56 pairs of imaginary eigenvalues of the Hamiltonian matrix were detected, with a maximum number of singular values exceeding the critical level equal to 10. We remark that this example is illustrative of a typical problem occurring in the generation of rational macromodels. Due to the presence of a few complex poles slightly outside the frequency band of the excitation pulse, the passivity violation outside this bandwidth can be significant. In this case the maximum singular value reaches the value of 1.08. Conversely, the in-band behavior is characterized by a very small violation (the largest in-band singular value is bounded by $\sigma_{\max} \simeq 1.001$. It should be kept in mind that a bandlimited excitation may only lead to the identification of a macromodel that is accurate in the tested frequency interval.

Algorithm 2 was applied to compensate passivity, reaching the goal in 30 iterations. The CPU time required for completing this task was 72 min (using a 2-GHz Pentium IV-based notebook). The CPU time needed for solving the Lyapunov (48) was about 6 s, while the solution of the least squares problem (61) required from 0.1 to 2 s per iteration, depending on the number of eigenvalues being perturbed. Therefore, most of the CPU time was required for the computation of the eigenvalues/eigenvectors of the Hamiltonian matrix, which in this case has size 1680. For a discussion on possible improvements and algorithm speedup see Section IV.C. The resulting singular values distribution is depicted in the right panel of Fig. 10. Some of the transient scattering responses of the passive macromodel are com-

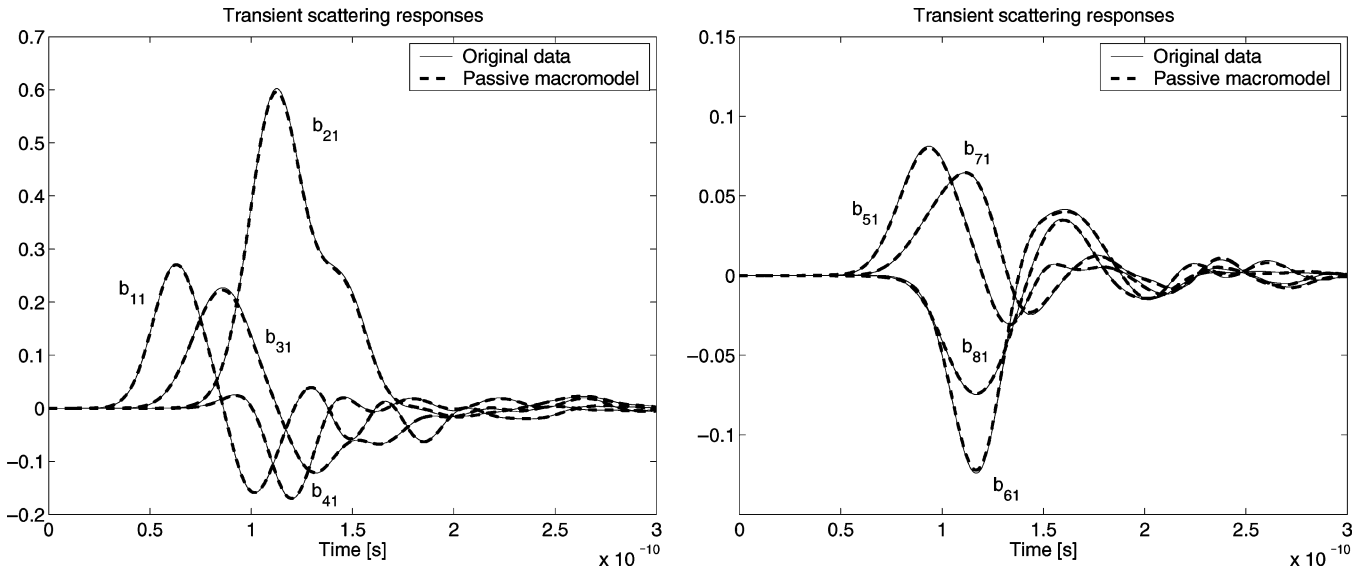

Fig. 11. Selected transient responses for the package structure of Fig. 9.

pared in Fig. 11 to the original responses obtained by the FDTD simulations, that were used for the identification of the macromodel. It is clear that passivity compensation did not degrade the accuracy in the approximation.

VI. Conclusion

We have presented a set of algorithms for the detection and correction of small passivity violations in minimal state-space realizations of linear multiport systems. All the algorithms presented here are based on spectral perturbations of some Hamiltonian matrices associated to the system. The presented algorithms find immediate application in the construction of passive macromodels for lumped/distributed interconnect networks which are known only through (frequency or time domain) input-output responses. Lumped macromodels are usually constructed by computing suitable rational approximations of the transfer matrices. Unfortunately, the direct state-space realization of such approximations often results nonpassive. However, if the approximation error is well under control, and if the original responses are representative of a passive structure, the passivity violations are small. With the denomination "small" we characterize those violations that can be compensated by applying small corrections to the nonpassive macromodel. In this case, the proposed algorithm results very efficient and guarantees that the passivity compensation is performed with the least impact on the input-output behavior of the system.

The main algorithms presented in this work are based on the assumption that the imaginary eigenvalues of the associated Hamiltonian matrices are simple or characterized by complete sets of eigenvectors. All the numerical examples that were investigated fall in this category. However, it is conceivable that in some applications the Hamiltonian matrix results defective. In such cases further investigations are needed for the precise characterization of the passivity violations. These investigations will be documented in a future study.

Acknowledgment

The author would like to thank Dr. Ruehli, IBM for providing some of the data that were used in the numerical examples, and his colleagues Prof. Canavero, Prof. Maio, and Dr. Stievano for many useful comments and suggestions.

References

[1] R. Achar and M. Nakhla, "Minimum realization of reduced-order high-speed interconnect macromodels," in *Signal Propagation on Interconnects*, H. Grabinski and P. Nordholz, Eds. Norwell, MA: Kluwer, 1998.

[2] V. Belevitch, *Classical Network Theory*. San Francisco, CA: Holden-Day, 1968.

[3] S. Boyd, V. Balakrishnan, and P. Kabamba, "A bisection method for computing the H_∞ norm of a transfer matrix and related problems," *Math. Control Signals Syst.*, vol. 2, pp. 207–219, 1989.

[4] S. Boyd, L. El Ghaoui, E. Feron, and V. Balakrishnan, *Linear Matrix Inequalities in System and Control Theory*. Philadelphia: SIAM, 1994.

[5] R. W. Brockett, *Finite Dimensional Linear Systems*. New York: Wiley, 1970.

[6] M. Celik, L. Pileggi, and A. Obadasioglu, *IC Interconnect Analysis*. Norwell, MA: Kluwer, 2002.

[7] W. D. C. Boaventura, A. Semlyen, M. R. Iravani, and A. Lopes, "Sparse network equivalent based on time-domain fitting," *IEEE Trans. Power Delivery*, vol. 17, pp. 182–189, Jan. 2002.

[8] S. Grivet-Talocia, F. Canavero, I. Maio, and I. Stievano, "Reduced-order macromodeling of complex multiport interconnects," in *URSI General Assembly*, Maastricht, Belgium, Aug. 19–23, 2002.

[9] S. Grivet-Talocia, "Enforcing passivity of macromodels via spectral perturbation of hamiltonian matrices," in *Proc. 7th IEEE Workshop Signal Propagation on Interconnects*, Siena, Italy, May 11–14, 2003, pp. 33–36.

[10] ——, "Package macromodeling via time-domain vector fitting," *IEEE Microwave Wireless Comp. Lett.*, vol. 13, pp. 472–474, Nov. 2003.

[11] ——, "Generation of passive macromodels from transient port responses," in *Proc. IEEE 12th Topical Meeting on Electrical Performance of Electronic Packaging*, Princeton, NJ, Oct. 27–29, 2003, pp. 287–290.

[12] B. Gustavsen and A. Semlyen, "Rational approximation of frequency domain responses by vector fitting," *IEEE Trans. Power Delivery*, vol. 14, pp. 1052–1061, July 1999.

[13] ——, "Enforcing passivity for admittance matrices approximated by rational functions," *IEEE Trans. Power Systems*, vol. 16, pp. 97–104, Feb. 2001.

[14] T. Kailath, *Linear Systems*. Englewood Cliffs, NJ: Prentice-Hall, 1980.

[15] P. Lancaster and L. Rodman, "Existence and uniquess theorems for the algebraic Riccati equation," *Int. J. Control*, vol. 32, no. 2, pp. 285–309, 1980.

[16] M. Nakhla and R. Achar, "Simulation of high-speed interconnects," *Proc. IEEE*, vol. 89, pp. 693–728, May 2001.
[17] R. Neumayer, A. Stelzer, F. Haslinger, and R. Weigel, "On the synthesis of equivalent-circuit models for multiports characterized by frequency-dependent parameters," *IEEE Trans. Microwave Theory Tech.*, vol. 50, pp. 2789–2796, Dec. 2002.
[18] A. E. Ruehli and A. C. Cangellaris, "Progress in the methodologies for the electrical modeling of interconnects and electronic packages," *Proc. IEEE*, vol. 89, pp. 740–771, May 2001.
[19] D. Saraswat, R. Achar, and M. Nakhla, "A fast algorithm and practical considerations for passive macromodeling of measured/simulated data," in *Proc. 11th IEEE Topical Meeting Electrical Performance of Electronic Packaging*, Monterey, CA, Oct. 21–23, 2002, pp. 297–300.
[20] ——, "Enforcing passivity for rational function based macromodels of tabulated data," in *Proc. 12th IEEE Topical Meeting Electrical Performance of Electronic Packaging*, Princeton, NJ, Oct. 27–29, 2003, pp. 295–298.
[21] A. Taflove, *Computational Electrodynamics: The Finite-Difference Time-Domain Method*. Norwood, MA: Artech House, 1995.
[22] C. F. Van Loan, "The ubiquitous Kronecker product," *J. Comput. Appl. Math.*, vol. 123, pp. 85–100, 2000.
[23] J. H. Wilkinson, *The Algebraic Eigenvalue Problem*. Oxford, U.K.: Oxford Univ. Press, 1965.
[24] J. C. Willems, "Least-squares stationary optimal control and the algebraic Riccati equation," *IEEE Trans. Automat. Control*, vol. AC-16, pp. 621–634, June 1971.

Stefano Grivet-Talocia (M'98) received the Laurea and the Ph.D. degrees in electronic engineering from the Polytechnic University of Turin, Turin, Italy.

From 1994 to 1996, he was at NASA/Goddard Space Flight Center, Greenbelt, MD, where he worked on applications of fractal geometry and wavelet transform to the analysis and processing of geophysical time series. Currently, he is an Associate Professor of Circuit Theory in the Department of Electronics, Polytechnic University of Turin. His current research interests are in numerical modeling of interconnects, applications of wavelets to computational electromagnetics, and passive macromodeling of lumped and distributed structures. He is author of more than 50 journal and conference papers.

Dr. Grivet-Talocia served as an Associate Editor for the IEEE TRANSACTIONS ON ELECTROMAGNETIC COMPATIBILITY from 1999 to 2001.